Electrophysiological characterization of a recombinant human Na^+-coupled nucleoside transporter (hCNT1) produced in *Xenopus* oocytes

Kyla M. Smith[1], Amy M. L. Ng[1], Sylvia Y. M. Yao[1], Kathy A. Labedz[1], Edward E. Knaus[3], Leonard I. Wiebe[3], Carol E. Cass[2,4], Stephen A. Baldwin[5], Xing-Zhen Chen[1], Edward Karpinski[1] and James D. Young[1]

Membrane Protein Research Group, Departments of [1]Physiology and [2]Oncology and Faculty of [3]Pharmacy, University of Alberta, Edmonton, Alberta T6G 2H7, Canada
[4]Cross Cancer Institute, Edmonton, Alberta T6G 2H7, Canada
[5]School of Biochemistry and Microbiology, University of Leeds, Leeds LS2 9JT, UK

Human concentrative nucleoside transporter 1 (hCNT1) mediates active transport of nucleosides and anticancer and antiviral nucleoside drugs across cell membranes by coupling influx to the movement of Na^+ down its electrochemical gradient. The two-microelectrode voltage-clamp technique was used to measure steady-state and presteady-state currents of recombinant hCNT1 produced in *Xenopus* oocytes. Transport was electrogenic, phloridzin sensitive and specific for pyrimidine nucleosides and adenosine. Nucleoside analogues that induced inwardly directed Na^+ currents included the anticancer drugs 5-fluorouridine, 5-fluoro-2′-deoxyuridine, cladribine and cytarabine, the antiviral drugs zidovudine and zalcitabine, and the novel thymidine mimics 1-(2-deoxy-β-D-ribofuranosyl)-2,4-difluoro-5-methylbenzene and 1-(2-deoxy-β-D-ribofuranosyl)-2,4-difluoro-5-iodobenzene. Apparent K_m values for 5-fluorouridine, 5-fluoro-2′-deoxyuridine and zidovudine were 18, 15 and 450 μM, respectively. hCNT1 was Na^+ specific, and the kinetics of steady-state uridine-evoked Na^+ currents were consistent with an ordered simultaneous transport model in which Na^+ binds first followed by uridine. Membrane potential influenced both ion binding and carrier translocation. The Na^+–nucleoside coupling stoichiometry, determined directly by comparing the uridine-induced inward charge movement to [^{14}C]uridine uptake was 1 : 1. hCNT1 presteady-state currents were used to determine the fraction of the membrane field sensed by Na^+ (61%), the valency of the movable charge (−0.81) and the average number of transporters present in the oocyte plasma membrane (6.8×10^{10} per cell). The hCNT1 turnover rate at −50 mV was 9.6 molecules of uridine transported per second.

(Resubmitted 19 May 2004; accepted after revision 4 June 2004; first published online 11 June 2004)
Corresponding author J. D. Young: 7–55 Medical Sciences Building University of Alberta, Edmonton, Alberta T6G 2H7, Canada. Email: james.young@ualberta.ca

Physiological nucleosides and nucleoside analogues have important biochemical, physiological and pharmacological activities in humans. Adenosine, for example, has cell-surface receptor-mediated functions in processes such as modulation of immune responses, platelet aggregation, renal function and coronary vasodilatation (Fredholm, 1997; Shryock & Belardinelli, 1997). Nucleoside analogues are commonly used in the therapy of cancer and viral infections (Handschumacher *et al.* 2000; Perigaud *et al.* 1994). Most nucleosides, including those with antineoplastic and/or antiviral activities are hydrophilic, and specialized plasma membrane nucleoside transporter (NT) proteins are often required for uptake into or release from cells (Baldwin *et al.* 1999; Mackey *et al.* 1999; Young *et al.* 2001). NT-mediated transport is therefore a critical determinant of metabolism and, for nucleoside drugs, their pharmacological actions.

Multiple nucleoside transport systems that differ in their cation dependence, permeant selectivities and inhibitor sensitivities have been observed in human and other mammalian cells and tissues (Cass, 1995; Griffiths & Jarvis, 1996; Young *et al.* 2001). The major *c*oncentrative systems (*cit*, *cif* and *cib*) are inwardly directed

 DOI: 10.1113/jphysiol.2004.068189

Na^+-dependent processes that have been described primarily in specialized cells, such as intestinal and renal epithelia, hepatocytes, choroid plexus, macrophages, splenocytes and leukaemic cells (Cass, 1995; Griffiths & Jarvis, 1996; Young *et al.* 2001). The equilibrative (bidirectional) transport processes (*es* and *ei*) mediate passive downhill transport of nucleosides, have generally lower permeant affinities than the concentrative systems and occur in most, possibly all, cell types (Cass, 1995; Griffiths & Jarvis, 1996; Young *et al.* 2001). Systems *cit* and *cif* are generally pyrimidine and purine nucleoside selective, respectively, whereas systems *cib*, *es* and *ei* transport both pyrimidine and purine nucleosides. The *es* process is inhibited by NBMPR (nitrobenzylthioinosine, 6-[(4-nitrobenzyl)thio]-9-β-D-ribofuranosylpurine), while system *ei* also transports nucleobases (Yao *et al.* 2002*b*).

Molecular cloning studies have resulted in the isolation and functional expression of cDNAs encoding the human and rodent proteins responsible for each of these nucleoside transport processes (Huang *et al.* 1994; Che *et al.* 1995; Yao *et al.* 1996*b*; Ritzel *et al.* 1997; Wang *et al.* 1997; Crawford *et al.* 1998; Ritzel *et al.* 1998, 2001). They belong to two unrelated and previously unrecognized protein families, the concentrative nucleoside transporter (CNT) and equilibrative nucleoside transporter (ENT) proteins. Their relationship to the processes defined by functional studies is: CNT1 (*cit*), CNT2 (*cif*), CNT3 (*cib*), ENT1 (*es*) and ENT2 (*ei*). Three further ENTs (ENT3, ENT4 and CLN3) of undetermined function have recently been identified (Hyde *et al.* 2001; Acimovic & Coe, 2002; Baldwin *et al.* 2004). Mammalian CNTs have 13 predicted transmembrane helices (TMs), with an intracellular N-terminus and an extracellular glycosylated C-terminus (Hamilton *et al.* 2001). NupC, an H^+-coupled CNT from *Escherichia coli*, has a similar predicted topology, but lacks TMs 1–3 (Craig *et al.* 1994; Hamilton *et al.* 2001). Other characterized CNTs include hfCNT from *Eptatretus stouti* (Loewen *et al.* 1999; Yao *et al.* 2002*a*), CeCNT3 from *Caenorhabditis elegans* (Xiao *et al.* 2001) and CaCNT from *Candida albicans* (Loewen *et al.* 2003).

Human CNT1 (hCNT1, 650 amino acid residues) (Huang *et al.* 1994) and rat CNT1 (rCNT1, 648 amino acid residues) (Ritzel *et al.* 1997) are 83% identical in amino acid sequence and have been studied functionally as recombinant proteins produced in *Xenopus* oocytes, *Saccharomyces cerevisiae* and cultured mammalian cells. Radioisotope flux studies have demonstrated pyrimidine nucleoside-selective (*cit*-type) Na^+-dependent fluxes of both ^3H- and ^{14}C-labelled physiological nucleosides and nucleoside drugs (Huang *et al.* 1994; Fang *et al.* 1996; Yao *et al.* 1996*a*,*b*; Ritzel *et al.* 1997; Mackey *et al.* 1998; Yao *et al.* 2001). In the present study, the two-microelectrode voltage-clamp technique was used to undertake an in-depth steady-state and presteady-state electrophysiological analysis of recombinant hCNT1 produced in *Xenopus* oocytes.

Methods

Heterologous expression in *Xenopus* oocytes

hCNT1 cDNA in pGEM-T (Ritzel *et al.* 1997; Loewen *et al.* 1999) or pGEM-HE (Ritzel *et al.* 2001) was linearized, respectively, with *Not*1 or *Nhe*1 and transcribed with T3 or T7 polymerase using the mMESSAGE mMACHINE$^{TM.}$ (Ambion, Austin, TX, USA) transcription system. Stage V–VI oocytes were isolated by collagenase treatment of ovarian lobes from female *Xenopus laevis* (Biological Sciences Vivarium, University of Alberta) that had been anaesthetized by immersion in 0.2% tricaine methanesulphonate (pH 7.4; Sigma, Oakville, ON, Canada). Frogs were humanely killed following final collection of oocytes in compliance with guidelines approved by the Canadian Council on Animal Care. Defolliculated oocytes were injected with 10 nl of water ± 10 ng of capped hCNT1 RNA transcript and incubated for 4 days at 18°C in modified Barth's solution (changed daily). The enhanced *Xenopus* expression vector pGEM-HE (Liman *et al.* 1992) produced greater hCNT1 functional activity than pGEM-T and was used in most experiments.

Steady-state electrophysiological studies

Oocyte membrane currents were measured using a GeneClamp 500B oocyte clamp (Axon Instruments, Inc., Foster City, CA, USA) in the two-electrode, voltage-clamp mode that was interfaced to an IBM compatible computer *via* a Digidata 1200A/D converter and controlled by pCLAMP software (Version 9.0, Axon Instruments, Inc.). Current signals were filtered at 20 Hz (four-pole Bessel filter) and sampled at a sampling interval of 20 ms. For data presentation, the signals were further filtered at 0.5 Hz by the pCLAMP program suite. Microelectrodes were filled with 3 M KCl and had resistances in the range 0.5–2.5 MΩ. All experiments were performed at room temperature (20°C) and oocytes were discarded if the membrane potential was unstable or more positive than −30 mV. Unless otherwise indicated, the membrane potential was clamped at a holding potential (V_h) of −50 mV and nucleoside was added at a concentration of

100 μM. The transport medium contained (mM): NaCl, 100; KCl, 2; $CaCl_2$, 1; $MgCl_2$, 1; Hepes, 10 (pH 7.5). In some experiments, Na^+ was replaced by equimolar choline.

Current–voltage (*I*–*V*) curves were determined from differences between steady-state currents generated in the presence and absence of permeant during 175 ms voltage pulses to potentials between −90 and +60 mV (10 mV increments). For *I*–*V* relations, the voltage rise time of the clamp was adjusted by use of an oscilloscope such that it varied between 200 and 500 μs. Currents were filtered at 2 kHz (four-pole Bessel filter) and sampled at a rate of 200 μs point^{-1} (corresponding to a sampling frequency of 5 kHz). The ability of H^+ to drive nucleoside transport was tested by replacing Na^+ in the transport medium with choline and varying the pH between 7.5 and 5.5 (10 mM MES (2-[*N*-morpholino]ethanesulphonic acid) was used in place of Hepes in solutions with pH values ≤ 6.5). Exposure of oocytes to acid pH was kept to intervals of < 2 min to minimize toxicity. For studies of phloridzin inhibition, currents were measured in the same oocyte before and after a 10 min preincubation with inhibitor (the time required for onset of maximum inhibition). Phloridzin remained present during uridine perfusion.

Current values are presented as means ± S.E.M. of 4 or more oocytes. Each experiment was repeated at least twice on oocytes from different frogs. Uridine kinetic parameters (apparent affinity, K_m^{uridine}; maximal current, $I_{\text{max}}^{\text{uridine}}$) were determined by current measurements at different uridine concentrations and analysed by least squares fits to the Michaelis-Menten eqn $I = I_{\text{max}}^{\text{uridine}}[\text{U}]/(K_m^{\text{uridine}} + [\text{U}])$, where *I* is the permeant-induced current and [U] represents the uridine concentration (SigmaPlot Version 4, Jandel Scientific Software, San Rafael, CA, USA). Kinetic parameters for other permeants were determined in similar fashion. The results from Na^+ activation experiments were fitted to the Hill equation, $I = I_{\text{max}}[\text{Na}^+]^n/(K_{\text{m}}^{\text{Na}^n} + [\text{Na}^+]^n)$, where *n* is the Hill coefficient, K_{m}^{Na} is the half-saturation constant for Na^+ activation, *I* is the uridine-induced steady-state current, and I_{max} is the predicted current maximum (SigmaPlot Version 4).

Radioisotope flux studies (phloridzin and β-DFP-5M inhibition)

Initial rates of hCNT1-mediated transport of 10 μM ^{14}C-labelled uridine (1 μCi ml^{-1}, Amersham Pharmacia Biotech, Canada) were measured at room temperature (1 min flux) as previously described (Huang *et al.* 1993; Ritzel *et al.* 1997). Values are presented as means ± S.E.M. of 10–12 oocytes, and each experiment was repeated at least twice on different batches of cells.

Cation–nucleoside coupling ratios

hCNT1 Na^+–nucleoside stoichiometry was determined by the simultaneous measurement of Na^+ current and [^{14}C]uridine influx under voltage-clamp conditions in the same oocyte (Chen *et al.* 1998; Loewen *et al.* 2003). Coupling ratios (± S.E.) were calculated from slopes of least-squares fits of uridine-dependent charge *versus* uridine accumulation for seven or more oocytes.

Presteady-state currents

Presteady-state currents were measured using a voltage step protocol. The membrane voltage was stepped using 250 ms voltage pulses from the holding potential (V_{h}) of −50 mV to a series of test potentials (V_{t}) ranging from −170 to +130 mV (20 mV increments). In experiments to determine the turnover rate of the transporter, membrane voltage was stepped from V_{h} of −50 mV to V_{t} from −170 to +150 mV in 40 mV increments to ensure maximal charge displacement while reducing the number of voltage pulses to which the oocyte was subjected. The maximal steady-state inward Na^+ current (I_{max}) was measured at V_{h} of −50 mV with a saturating concentration of uridine (100 μM). Currents were filtered and sampled as described for *I*–*V* relationships. For data presentation, the current at each test potential was averaged from five sweeps. If necessary, signals were further filtered at 750 Hz (pCLAMP 9.0). Presteady-state currents due to hCNT1 were fitted using the Chebyshev method with two exponential functions (pCLAMP 9.0). Since the capacitive transients were longer than 1–2 ms, amplitudes were extrapolated to 1 ms after the onset of the step. Current–time integrals were calculated using these extrapolated amplitude values. Curve fits were considered successful only if the correlation coefficient (*r*) was 0.95 or higher. Charge movements (*Q*) obtained from the current-time integral of the curve fits were plotted against voltage and fitted to the Boltzmann function:

$$(Q - Q_{\text{hyp}})/Q_{\text{T}} = 1/[1 + \exp(z_{\text{d}}(V_{\text{t}} - V_{0.5})F/RT)]$$

where the total charge $Q_{\text{T}} = Q_{\text{dep}} - Q_{\text{hyp}}$ (Q_{dep} and Q_{hyp} representing *Q* at depolarizing and hyperpolarizing limits, respectively), z_{d} is the product of the valency of the charge (*z*) and the apparent fraction of the field (δ) sensed by that charge, V_{t} is the membrane voltage during the pulse, $V_{0.5}$ is the membrane voltage at which half of the total charge has moved, *F* is Faraday's constant, *R* is the gas constant and T is the absolute temperature (Hazama *et al.* 1997). Mean values of $V_{0.5}$ and z_d (± S.E.M.) were determined from individual Boltzmann fits to data from three to six separate experiments in different oocytes.

Chemicals

Nucleosides, nucleoside analogues and phloridzin were purchased from Sigma (Oakville, ON, Canada). β-DFP-5M 1-(2-deoxy-β-D-ribofuranosyl-2,4-difluoro-5-methylbenzene) and β-DFP-5I (1-(2-deoxy-β-D-ribofuranosyl)-2,4-difluoro-5-iodobenzene) were synthesized as previously described (Wang *et al.* 2001).

Results

General characteristics

Measured in *Xenopus* oocytes at $V_h = -50$ mV and using choline as Na^+ substitute, transport of uridine by recombinant hCNT1 was electrogenic, Na^+ dependent and H^+ independent (shown in Fig. S1 in Supplementary material, available online). In contrast to reports for h/rCNT1 by other investigators (Dresser *et al.* 2000; Lostao *et al.* 2000), addition of permeant to hCNT1-producing oocytes in the absence of Na^+ did not generate any detectable inward current (Fig. S1, Supplementary material). This agrees with previous radiotracer uptake studies that found only very small amounts of nucleoside uptake in the absence of Na^+ (Huang *et al.* 1994; Ritzel *et al.* 1997). This minor component of Na^+-independent transport had the characteristics of 'slippage' (i.e. uncoupled nucleoside transport) and would not be expected to be electrogenic. hCNT1 steady-state currents were voltage dependent and increased at more negative potentials (Fig. S2, Supplementary material). Currents approached zero, but did not reverse polarity at potentials up to +60 mV. No steady-state currents were observed in control water-injected oocytes.

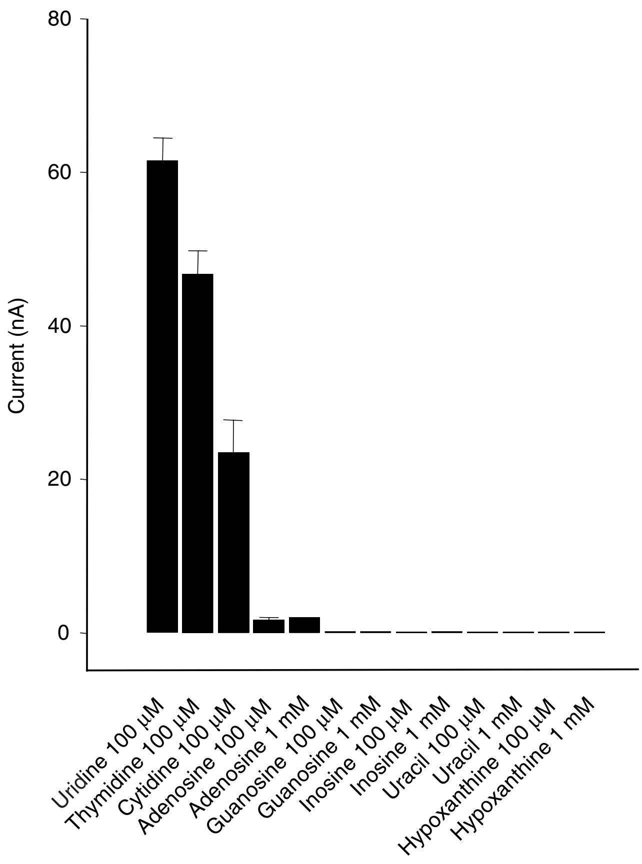

Figure 1. Nucleoside specificity of hCNT1
The permeant selectivity of hCNT1 was investigated in Na^+-containing transport medium by measuring the currents evoked by a variety of pyrimidine (100 μM) and purine (100 μM and 1 mM) nucleosides. The nucleobases uracil and hypoxanthine (100 μM and 1 mM) were also tested. hCNT1-mediated currents are expressed as the mean ± S.E.M. of 3–4 different oocytes. The expression vector was pGEM-HE.

Transport of physiological nucleosides

hCNT1 selectivity for pyrimidine nucleosides has been demonstrated previously using conventional radioisotope flux measurements (Ritzel *et al.* 1997). It has also been found that hCNT1 and rCNT1 mediate low, but significant radioisotope fluxes of adenosine, but not of inosine or guanosine (Huang *et al.* 1994; Fang *et al.* 1996; Yao *et al.* 1996*b*; Ritzel *et al.* 1997; Loewen *et al.* 1999). These results were confirmed and extended in Fig. 1 using electrophysiological techniques. hCNT1 currents elicited by application of test permeants in Na^+-containing transport medium were: uridine, thymidine, cytidine (100 μM) > adenosine (100 μM and 1 mM); guanosine and inosine (100 μM and 1 mM) were without effect. The nucleobases of uridine (uracil) and inosine (hypoxanthine) (100 μM and 1 mM) were also not transported. No currents were observed in control water-injected oocytes (data not shown). Therefore, hCNT1 is specific for pyrimidine nucleosides and adenosine. In agreement with radiotracer uptake measurements (Ritzel *et al.* 1997), adenosine elicited larger currents than 2′-deoxyadenosine (Fig. 2*B*).

In radioisotope flux studies, adenosine is transported by rCNT1 with a similar apparent K_m to uridine (~30 μM), but with a much lower V_{max} due to slow conversion of the CNT1–adenosine complex from outward-facing to inward-facing conformations (Yao *et al.* 1996*b*). Competition experiments were undertaken with hCNT1 to determine if the same kinetic behaviour could be demonstrated electrophysiologically.

As shown in Fig. S3 (Supplementary material) the current produced by a saturating concentration of uridine was substantially higher than that produced in the same oocyte by simultaneous perfusion of both uridine and adenosine.

Transport of nucleoside analogues

We also used electrophysiology to determine transportability of 100 μM and 1 mM concentrations of a panel of clinically important antiviral and anticancer nucleoside drugs and other nucleoside analogues (Fig. 2). Large to moderate inward currents were elicited by application of 2′-deoxyuridine, 2′,3′-dideoxyuridine, 5-fluorouridine, 5-fluoro-2′-deoxyuridine, zalcitabine (ddC, 2′,3′-dideoxycytidine) and zidovudine (AZT, 3′-azido-3′-deoxythymidine) (Fig. 2*A*). Smaller, but significant inward currents were also observed for cladribine (2-chloro-2′-deoxyadenosine) (Fig. 2*B*). Cytarabine (1-β-D-arabinofuranosylcytosine) and tubercidin (7-deazaadenosine) generated small inward

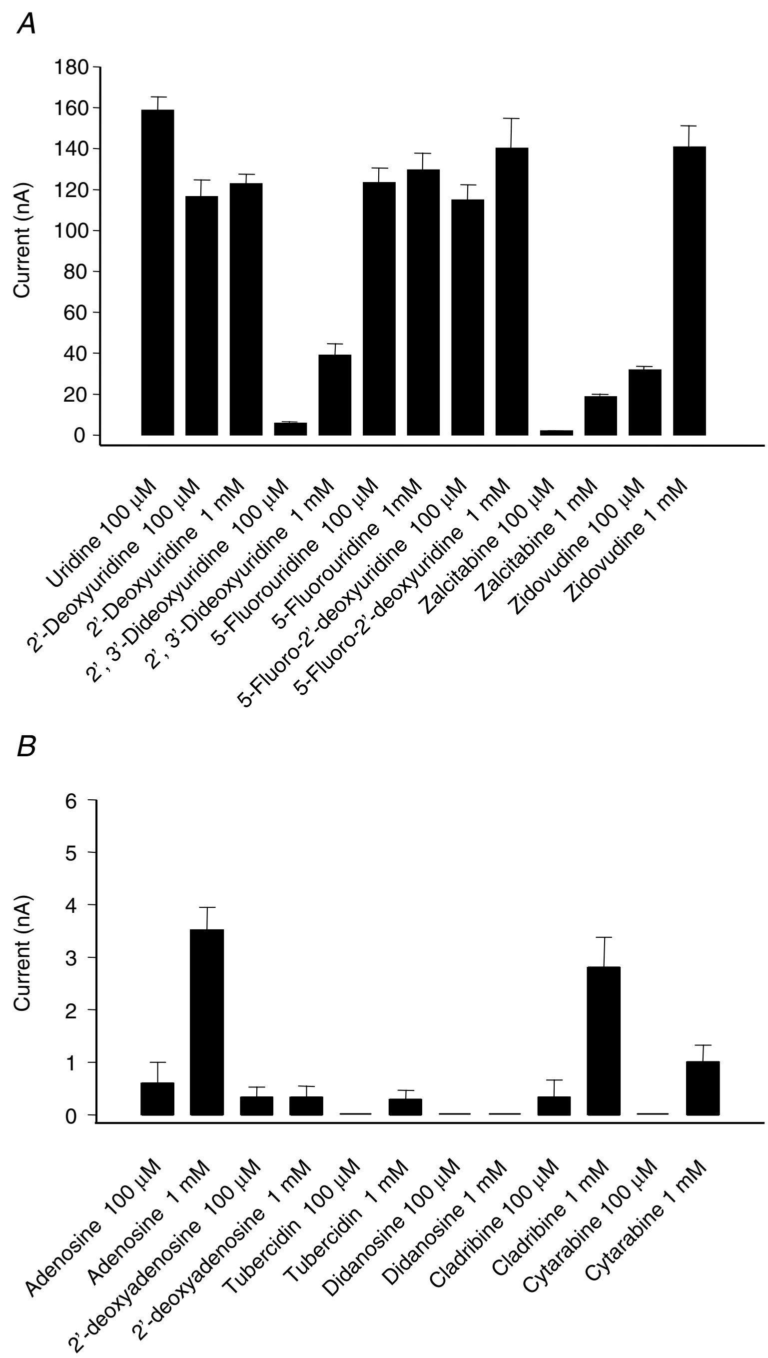

Figure 2. Transport of nucleoside analogues and nucleoside drugs by hCNT1
Current responses generated by perfusing hCNT1-producing oocytes with various pyrimidine and purine nucleoside analogues and nucleoside drugs (100 μM and 1 mM) in Na^+-containing medium (*A* and *B*). Values are means ± S.E.M. for 5–6 different oocytes. The same experiment was also performed in control water-injected oocytes (data not shown); no inward currents were generated. The expression vector was pGEM-HE.

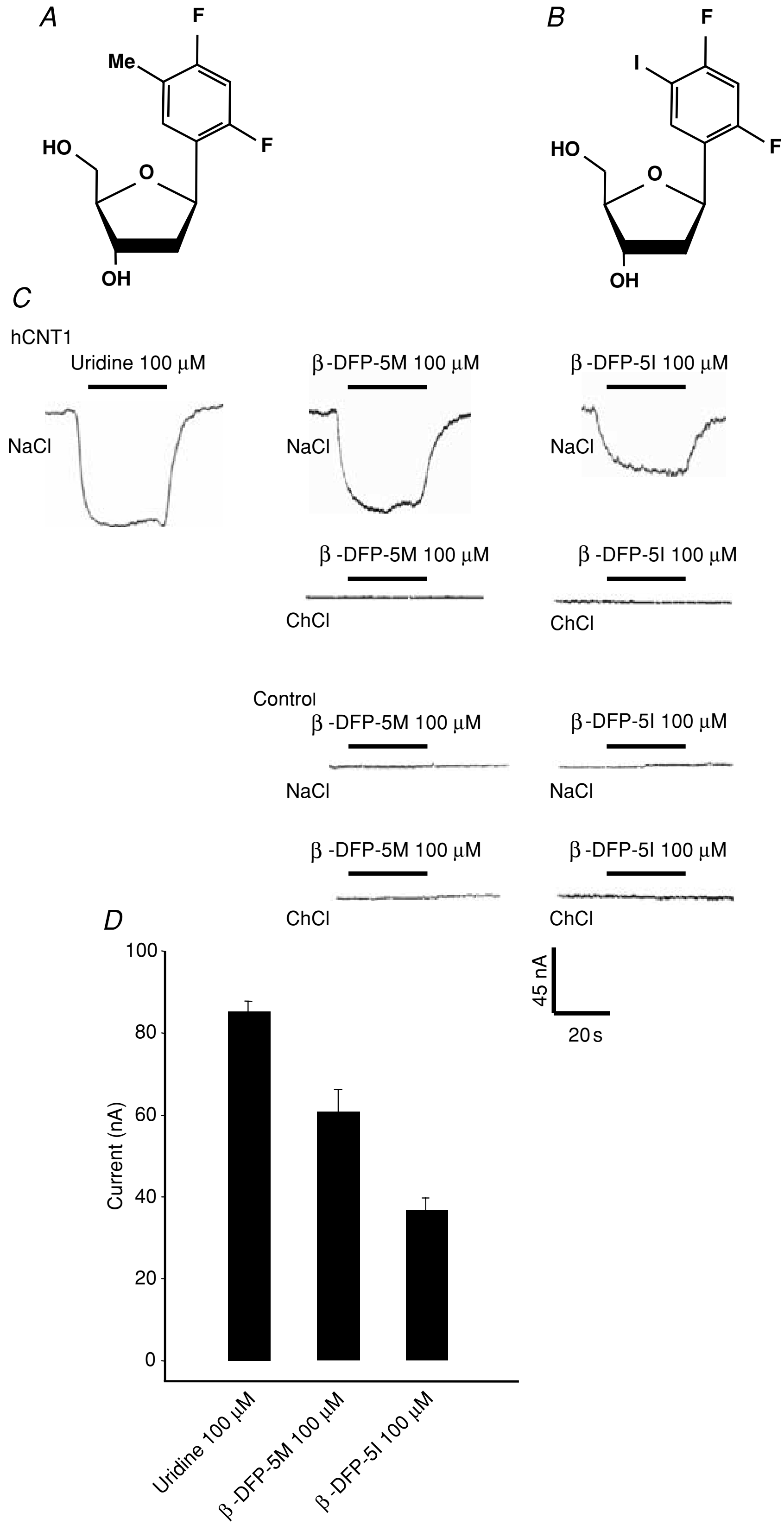

Figure 3. Transport of thymidine mimetics by hCNT1

A, structure of β-DFP-5M (1-(2-deoxy-β-D-ribofuranosyl)-2,4-difluoro-5-methylbenzene). *B*, structure of β-DFP-5I (1-(2-deoxy-β-D-ribofuranosyl)-2,4-difluoro-5-iodobenzene). *C*, oocytes were injected with 10 nl of water without (control) or with 10 ng of hCNT1 RNA transcript. The expression vector was pGEM-HE. Current responses were generated by perfusing individual hCNT1-producing oocytes with either 100 μM β-DFP-5M or β-DFP-5I in Na^+- or choline-containing transport medium (top panel). The current produced by 100 μM uridine in Na^+-containing medium is shown for comparison. The same experiment was performed in a control water-injected oocyte (bottom panel). *D*, a comparison of hCNT1-mediated currents following addition of 100 μM uridine, β-DFP-5M or β-DFP-5I in Na^+-containing medium. Values are means ± S.E.M. for 3 different oocytes.

currents only at the higher permeant concentration of 1 mM, while didanosine (ddI, 2′, 3′-dideoxyinosine) was without effect (Fig. 2*B*). As illustrated for zidovudine in Fig. S4 (Supplementary material), currents were reversible and abolished in Na^+-free medium. No currents were observed in control water-injected oocytes.

Transport of nucleoside mimics

The novel thymidine mimetics β-DFP-5M and β-DFP-5I (Fig. 3*A* and *B*, respectively), in which the pyrimidine base was replaced by a substituted aromatic ring, were similarly tested as potential hCNT1 permeants. Both compounds induced reversible, Na^+-dependent inward currents in hCNT1-producing oocytes, but not in control water-injected oocytes (Fig. 3*C* and *D*). β-DFP-5M inhibited hCNT1-mediated ^{14}C-labelled uridine influx with an IC_{50} value (± S.E.) of 0.56 ± 0.06 mM ($r = 0.99$) (Fig. S5, Supplementary material).

Na^+ and uridine steady-state kinetics: order of binding

When the dependence of hCNT1-mediated Na^+ currents on uridine concentration (0–1000 μM) was examined at three different extracellular Na^+ concentrations (5, 25 and 100 mM), saturable inward current responses that were consistent with simple Michaelis-Menten kinetics were observed (Fig. 4*A*). At 5, 25 and 100 mM external Na^+, the apparent affinity for uridine increased as $[Na^+]_{out}$ increased, with no significant change in the maximal current, yielding apparent $K_m^{uridine}$ values (± S.E.) of 139 ± 10, 80 ± 7 and 32 ± 5 μM, respectively, with $I_{max}^{uridine}$ values (± S.E.) of 54 ± 1, 55 ± 2 and 54 ± 2 nA, respectively. The corresponding dependence of hCNT1-mediated Na^+ currents on the external concentration of Na^+ (0–100 mM) was examined at two different concentrations of extracellular uridine (25 and 100 μM) (Fig. 4*B*). The Na^+ concentration dependence of the steady-state transport current also conformed to simple Michaelis-Menten kinetics. Both the apparent affinity of the transporter for Na^+ and the maximal current increased when the external concentration of uridine increased. At 25 and 100 μM uridine, apparent K_m^{Na} values (± S.E.) were 12 ± 2 and 3 ± 1 mM, respectively, with I_{max}^{Na} values (± S.E.) of 38 ± 2 and 64 ± 3 nA, respectively.

Together, the data in Fig. 4*A* and *B* indicate a sequential ordered binding mechanism in which Na^+ binds to the transporter first, increasing its affinity for the nucleoside, which then binds second (Jauch & Lauger, 1986; Stein,

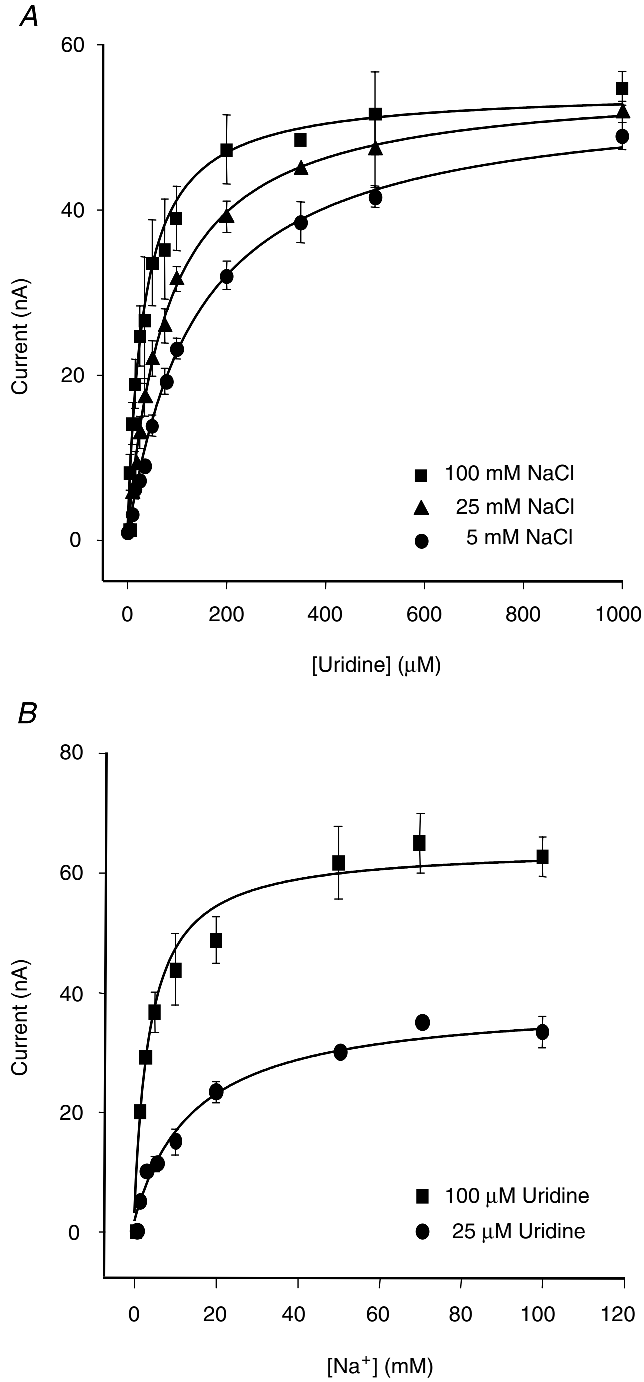

Figure 4. Steady-state hCNT1 kinetics and the order of solute binding
A, the dependence of hCNT1-mediated currents on the external concentration of uridine (0–1000 μM) was examined at three different concentrations of Na^+ (5, 25 and 100 mM). hCNT1-mediated currents are expressed as the mean ± S.E.M. of 5–6 different oocytes. *B*, the dependence of hCNT1-mediated currents on the external concentration of Na^+ (0–100 mM) was examined at 25 and 100 μM uridine. hCNT1-mediated currents are expressed as the mean ± S.E.M. of 4–5 different oocytes. The expression vector was pGEM-T.

1990; Klamo *et al.* 1996; Mackenzie *et al.* 1996*b*). Transport of nucleoside and ion is simultaneous because decreasing the concentration of either Na^+ or uridine decreased the apparent affinity of the other (Eskandari *et al.* 1997). A sequential ordered binding mechanism is consistent with studies of native *cit* and *cif* transport activity in bovine renal brush-border membrane vesicles showing that the apparent affinity for nucleoside increased as the external Na^+ concentration was raised (Williams & Jarvis, 1991). The predicted hCNT1 Na^+–nucleoside coupling ratio was 1 : 1, since fitting the 25 and 100 μM uridine current data of Fig. 4*B* to the Hill equation yielded Hill coefficients ($\pm$ s.e.) of 0.90 $\pm$ 0.12 and 0.79 $\pm$ 0.06, respectively.

Na^+ and uridine steady-state kinetics: voltage dependence

We also used steady-state kinetics to investigate the mechanism behind hCNT1 voltage dependence. The apparent affinities for Na^+ (K_m^{Na}) and uridine ($K_m^{uridine}$) and corresponding I_{max} values were measured at four different holding potentials ($V_h = -10$, -30, -50 and -70 mV) (curves not shown). K_m^{Na} was determined at an external uridine concentration of 100 μM, while $K_m^{uridine}$ was determined at both 10 and 100 mM external Na^+. $K_m^{uridine}$ was unaffected by membrane potential at 100 mM Na^+, but was voltage dependent at 10 mM Na^+, decreasing from 84 to 44 μM as the membrane potential was increased from -10 to -70 mV. At high negative membrane potentials therefore $K_m^{uridine}$ (10 mM Na^+) approached that observed at 100 mM external Na^+, indicating that the voltage dependence of $K_m^{uridine}$ is the result of voltage dependence of Na^+ binding (Birnir *et al.* 1991; Parent *et al.* 1992*a*). Consistent with this conclusion, we found that K_m^{Na} was voltage sensitive, decreasing from 5 to 1 mM as the membrane potential was varied from -10 to -70 mV. $I_{max}^{uridine}$ and I_{max}^{Na} also showed voltage dependence, their magnitudes increasing as the membrane potential was made more negative. Membrane potential therefore influences both ion-binding and carrier translocation (Birnir *et al.* 1991; Parent *et al.* 1992*a*).

Na^+ and uridine steady-state kinetics: phloridzin inhibition

Figure S6 (Supplementary material) demonstrates phloridzin inhibition of uridine currents in hCNT1-producing oocytes. Inhibition was partial (~80%), even at high phloridzin concentrations, and the IC_{50} value for inhibition of the phloridzin-sensitive component of current was 0.21 $\pm$ 0.05 mM ($r = 0.98$). A similar inhibition profile was obtained for ^{14}C-labelled uridine influx (IC_{50} of 0.35 $\pm$ 0.12 mM; $r = 0.99$) (Fig. S6, Supplementary material). In kinetic experiments, phloridzin (5 mM) reduced both $I_{max}^{uridine}$ and I_{max}^{Na}, but had opposite effects on $K_m^{uridine}$ and K_m^{Na} (Fig. 5). $K_m^{uridine}$ and $I_{max}^{uridine}$ values ($\pm$ s.e.) (100 mM NaCl) were 22 $\pm$ 3 μM and 151 $\pm$ 5 nA, respectively, in the absence of phloridzin, and 131 $\pm$ 27 μM and 73 $\pm$ 9 nA, respectfully, in the presence of phloridzin (Fig. 5*A*). Corresponding K_m^{Na} and I_{max}^{Na} values ($\pm$ s.e.) (100 μM uridine) were 3.0 $\pm$ 0.3 mM and 95 $\pm$ 2 nA, respectively, in the absence of phloridzin, and 0.8 $\pm$ 0.2 mM and 22 $\pm$ 1 nA, respectively, in the presence of phloridzin (Fig. 5*B*). The Hill coefficient ($\pm$ s.e.) for the control data in Fig. 5*B* was 1.1 $\pm$ 0.1.

Nucleoside analogue steady-state kinetics

Nucleoside analogues from Fig. 2*A* exhibiting robust steady-state currents were analysed kinetically as shown in Fig. S7 (Supplementary material). Apparent K_m and I_{max} (100 mM NaCl) values derived from these data are compared to uridine in Table 1. Relative affinities were in the order 5-fluoro-2′-deoxyuridine, 5-fluorouridine > uridine, 2′-deoxyuridine ≫ zidovudine, with calculated $I_{max} : K_m$ ratios (a measure of transport efficiency) highest for uridine and 2′-deoxyuridine. The hCNT1 zidovudine apparent K_m of 0.45 mM is in good agreement with values determined for rCNT1 transport of zidovudine and zalcitabine by radioisotope flux studies (Yao *et al.* 1996*a*).

Cation–nucleoside coupling ratio

The stoichiometry of Na^+–uridine cotransport was determined in individual hCNT1-producing oocytes by simultaneously measuring uridine-evoked hCNT1 current and [^{14}C]uridine uptake under voltage-clamp conditions (Fig. 6). Figure 6*A* is a representative uridine-dependent current recording (200 μM [^{14}C]uridine, 100 mM NaCl) in an hCNT1-producing oocyte clamped at -50 mV. Current reached an initial maximal value and then progressively decreased, a phenomenon that has also been observed for other cotransporters and is thought to result from (i) decreased ion concentrations in the immediate vicinity of the extracellular membrane, and (ii) *trans*-inhibition of transport activity by the accumulation of intracellular permeants and/or ions (Chen *et al.* 1998; Mackenzie *et al.* 1998; Chen *et al.* 1999). Results for groups of seven to nine different oocytes at holding potentials of -30, -50 and -90 mV yielded linear plots of charge (pmol) *versus* uptake (pmol), the slopes of which were independent of voltage and equal to the Na^+–nucleoside coupling ratio (Fig. 6*B*–*D*). At $V_h = -30$ mV, the linear correlation between uridine-dependent charge and uridine accumulation gave a stoichiometry (± S.E.) of 0.92 ± 0.15 (Fig. 6*B*), compared to 0.89 ± 0.02 at −50 mV (Fig. 6*C*) and 0.90 ± 0.09 at −90 mV (Fig. 6*D*).

Presteady-state currents of hCNT1

Unless otherwise specified, presteady-state experiments were performed in the absence of nucleoside to eliminate steady-state inward currents of hCNT1 and to isolate partial reactions of the transport cycle. Oocytes were voltage clamped at a holding potential (V_h) of −50 mV, and presteady-state currents were activated by voltage steps to a series of test potentials (V_t). Figure S8 (Supplementary material) shows representative total current recordings in an hCNT1-producing oocyte bathed in 100 mM Na^+-containing transport medium. Current relaxations, which persisted for tens of milliseconds after the time required to charge the membrane capacitance, were apparent in both the ON response, when V_h was stepped to V_t, and in the OFF response, when V_t was returned to V_h. These relaxations were also observed in hCNT1-producing oocytes in the absence of external Na^+, but were not seen in control water-injected oocytes (Fig. S8, Supplementary material). In the presence of external Na^+, the charge movement at the onset of the voltage pulse (Q_{ON}) was found to be equal and opposite to that at the return to the prepulse potential (Q_{OFF}), demonstrating conservation of charge during ON and OFF voltage steps (Fig. S9, Supplementary material). Figure 7*A* shows Q_{OFF}, normalized to Q_T, in a representative hCNT1-producing oocyte plotted as a function of voltage (25 mM NaCl). The *Q*–*V* relation obeyed a Boltzmann function, reversing at V_h and approaching saturation with both hyperpolarization and depolarization. The experiment was repeated in five different oocytes and at three additional Na^+ concentrations (10, 50 and 100 mM NaCl). Mean values of z_d (± S.E.M.) from individual Boltzmann fits were unaffected by Na^+ concentration (−0.47 ± 0.04, −0.51 ± 0.03, −0.50 ± 0.04 and −0.50 ± 0.02 at 10, 25, 50 and 100 mM external NaCl, respectively), and similar to those that can be calculated from the data of Larráyoz *et al.* (2004), while estimates of $V_{0.5}$, plotted *versus* the log of Na^+ concentration, shifted towards more negative potentials as the concentration of Na^+ was reduced (Fig. 7*B*). The fitted line corresponded to a shift (± S.E.) of 41 ± 1 mV for an e-fold change in Na^+ concentration, and was converted to the effective fraction

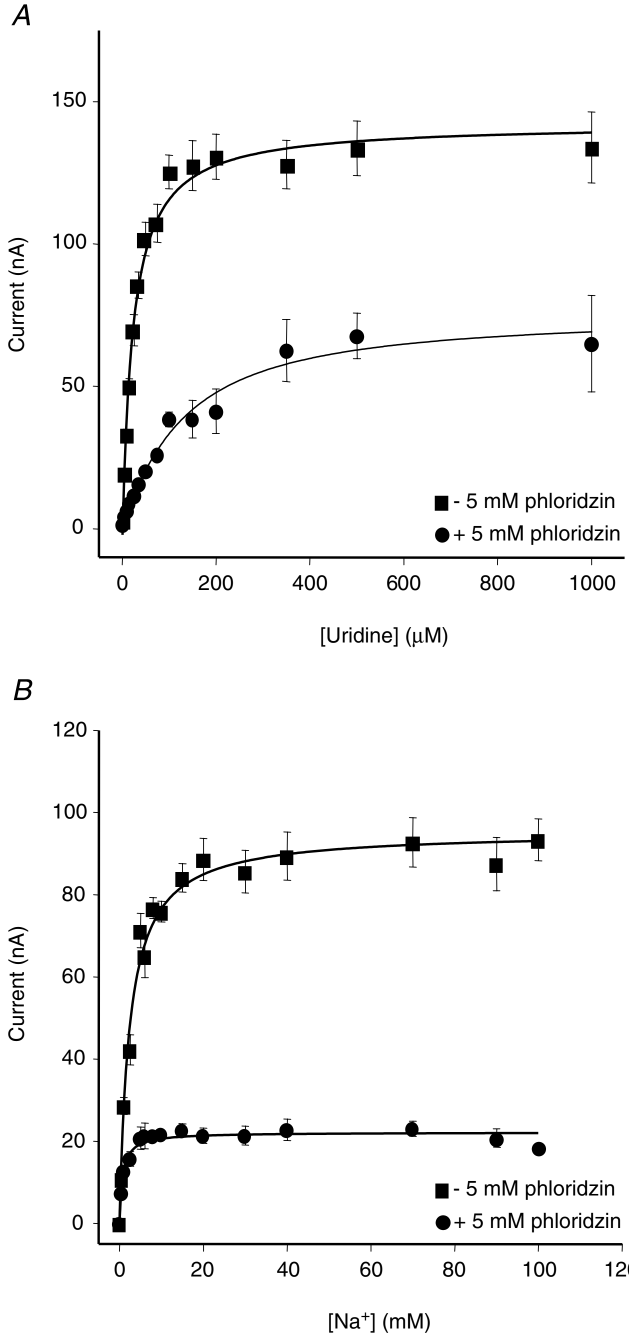

Figure 5. Effect of phloridzin on hCNT1 steady-state kinetics
A, uridine-induced currents (0–1000 μM) in hCNT1-producing oocytes were measured in Na^+-containing transport medium (100 mM NaCl) before and after incubation with 5 mM phloridzin. Currents are expressed as the mean ± S.E.M. of 5–6 different oocytes. *B*, uridine-induced currents (100 μM) in hCNT1-producing oocytes were measured in the presence of increasing concentrations of external Na^+ (0–100 mM) before and after incubation with 5 mM phloridzin. Currents are expressed as the mean ± S.E.M. of 5–6 different oocytes. The expression vector was pGEM-HE.

Table 1. Kinetic properties of hCNT1

Permeant	Apparent K_m[a] (μM)	I_{max}[a] (nA)	$I_{max} : K_m$	Turnover rate (s^{-1})
Uridine	22 ± 3	151 ± 5	6.9	9.6[b]
2′-Deoxyuridine	23 ± 4	172 ± 3	7.5	10.9[c]
5-Fluorouridine	18 ± 3	67 ± 1	3.7	4.3[c]
5-Fluoro-2′-deoyxuridine	15 ± 2	61 ± 1	4.1	3.9[c]
Zidovudine	450 ± 28	221 ± 5	0.5	14.1[c]

[a]From Figs 5*A* and S7 (Supplementary material). [b]Calculated from Fig. 8. [c]Calculated from I_{max} value relative to uridine.

of the electric field (δ) sensed by Na^+ using the relationship $\delta = kT/(e_o \times 41\ \mathrm{mV})$, where k is the Boltzmann constant and e_o is the elementary charge (Mager *et al.* 1993). The value of δ was 61 ± 1%, and implies binding of sodium to site(s) that traverse ~61% of the membrane electric field. The valency of the moveable charge (z), calculated from the relationship $z_d = \delta z$, was −0.81 ± 0.03, consistent with the transporter having one net negative charge. The effects of uridine (0–100 μM) on hCNT1 presteady-state currents and on Q_T (calculated for the OFF response) were also examined (Fig. S10, Supplementary material). External uridine increased the hCNT1 steady-state uridine-induced current (100 mM NaCl), but reduced presteady-state currents and Q_T. At 25 μM uridine, a concentration close to the uridine apparent $K_m^{uridine}$, Q_T was decreased by ~50%. Adenosine also has the ability to inhibit hCNT1 presteady-state currents (Larráyoz *et al.* 2004).

We also used the Boltzmann parameters to estimate the turnover rate (also known as turnover number) of hCNT1 and the number of transporter molecules present in the oocyte plasma membrane (Loo *et al.* 1993; Panayotova-Heiermann *et al.* 1995; Wadiche *et al.* 1995). Linear regression analysis of the steady-state transport current (100 mM NaCl) at a saturating concentration of uridine (100 μM) at −50 mV (I_{max}) *versus* Q_T (calculated for the OFF response) in oocytes with differing levels of hCNT1 expression yielded a straight line with a slope (± S.E.) of 17.2 ± 4.4 s^{-1}, corresponding to a charge transfer rate (Φ) of 8.6 ± 2.2 s^{-1} (slope × z_d = 17.2 × 0.50) (Fig. 8) (Wadiche *et al.* 1995). Since the turnover rate of the transporter is given by Φ/ν (Wadiche *et al.* 1995), where ν is the number of fundamental charges translocated per molecule of uridine and equals the Na^+–uridine coupling ratio (−50 mV) of 0.89 ± 0.02 (Fig. 6*C*), the number of uridine molecules transported per hCNT1 protein per second was 9.6 ± 2.5 s^{-1}. The numbers of recombinant hCNT1 transporters expressed in the oocyte plasma membrane (N), determined from Fig. 8 and the equation $Q_T = Ne_oz_d$ (Wright *et al.* 1994; Klamo *et al.* 1996; Eskandari *et al.* 1997), were in the range (5.4–8.5) × 10^{10} per oocyte, with a mean value (± S.E.M.) of (6.8 ± 0.2) × 10^{10}.

Discussion

Na^+-dependent hCNT1 (Ritzel *et al.* 1997), the prototypic human member of the CNT family of nucleoside transport proteins, is responsible for the concentrative cellular uptake of both physiological nucleosides and clinically important anticancer and antiviral nucleoside drugs. In immunolocalization studies, the rat orthologue of hCNT1 (rCNT1) is expressed predominantly in the brush-border membranes of the polarized epithelial cells of jejunum and renal cortical tubules, and in the bile canalicular membranes of liver parenchymal cells (Hamilton *et al.* 2001). In the present study, we have used the two-electrode voltage clamp in combination with heterologous expression in *Xenopus* oocytes to undertake steady-state and presteady-state electrophysiological studies of recombinant hCNT1.

Transport of nucleosides by hCNT1 was electrogenic and specific for pyrimidine nucleosides and adenosine. The latter nucleoside functions as a high-affinity low-capacity permeant, allowing it to act, in appropriate circumstances, as an hCNT1 inhibitor. Inosine, guanosine and nucleobases were not transported, even at high concentrations. Together with previous radioisotope flux studies and our parallel electrophysiological studies of rCNT1 (data not shown), the present findings contradict reports that adenosine is not transported by either hCNT1 or rCNT1 (Dresser *et al.* 2000; Larráyoz *et al.* 2004). Consistent with a physiological role of hCNT1 in renal handling of nucleosides, larger currents were elicited by adenosine (which is reabsorbed) than with 2′-deoxyadenosine (which is excreted).

Radioisotope flux studies have provided evidence that hCNT1 and rCNT1 also transport various nucleoside analogues, including clinically important nucleoside drugs with antineoplastic and/or antiviral activities (Huang *et al.* 1994; Fang *et al.* 1996; Yao *et al.* 1996*a*,*b*; Ritzel *et al.* 1997; Mackey *et al.* 1998; Yao *et al.* 2001). In the present study, inward currents were observed with the anticancer drugs 5-fluorouridine and 5-fluoro-2′-deoxyuridine, and with the antiviral drugs zidovudine and zalcitabine. Both fluorinated compounds were well tolerated (K_m values ~15 μM). Unlike adenosine and 2′-deoxyadenosine, lack of the C(2′)-OH in 5-fluoro-2′-deoxyuridine compared to 5-fluorouridine had no discernable effect on transport, a finding confirmed by kinetic comparisons between the two parent compounds 2′-deoxyuridine and uridine. Similarly, gemcitabine, an anticancer analogue of 2′-deoxycytidine, is also a good hCNT1 permeant (apparent K_m ~25 μM) (Mackey *et al.* 1999). In contrast, absence of the C(3′)-OH in zidovudine (and zalcitabine) resulted in a > 10-fold decrease in transportability. The zidovudine K_m of 0.45 mM exceeds therapeutic levels of zidovudine in plasma, but is consistent with a role of hCNT1 in intestinal absorption of the drug during oral administration. Smaller inward currents were observed with the anticancer nucleoside drugs cladribine (an analogue of adenosine) and cytarabine (an analogue of cytidine). One millimolar cytarabine was required to produce a detectable inward current, suggesting that it functions as a low-affinity hCNT1 permeant, a conclusion supported by radiotracer flux studies in transfected mammalian cells, where 0.5 mM cytarabine caused only partial inhibition of uridine transport activity (Graham *et al.* 2000).

Two novel pyrimidine nucleoside mimics (β-DFP-5M and β-DFP-5I) (Wang *et al.* 2001) also functioned as low-affinity hCNT1 permeants. These compounds demonstrate that the pyrimidine ring is not required for translocation by hCNT1. The ability of the aromatic ring of β-DFP-5M and β-DFP-5I to functionally substitute for the pyrimidine moiety of nucleosides indicates that π–π interactions corresponding to those documented for trypanosomal ENT proteins (de Koning & Jarvis,

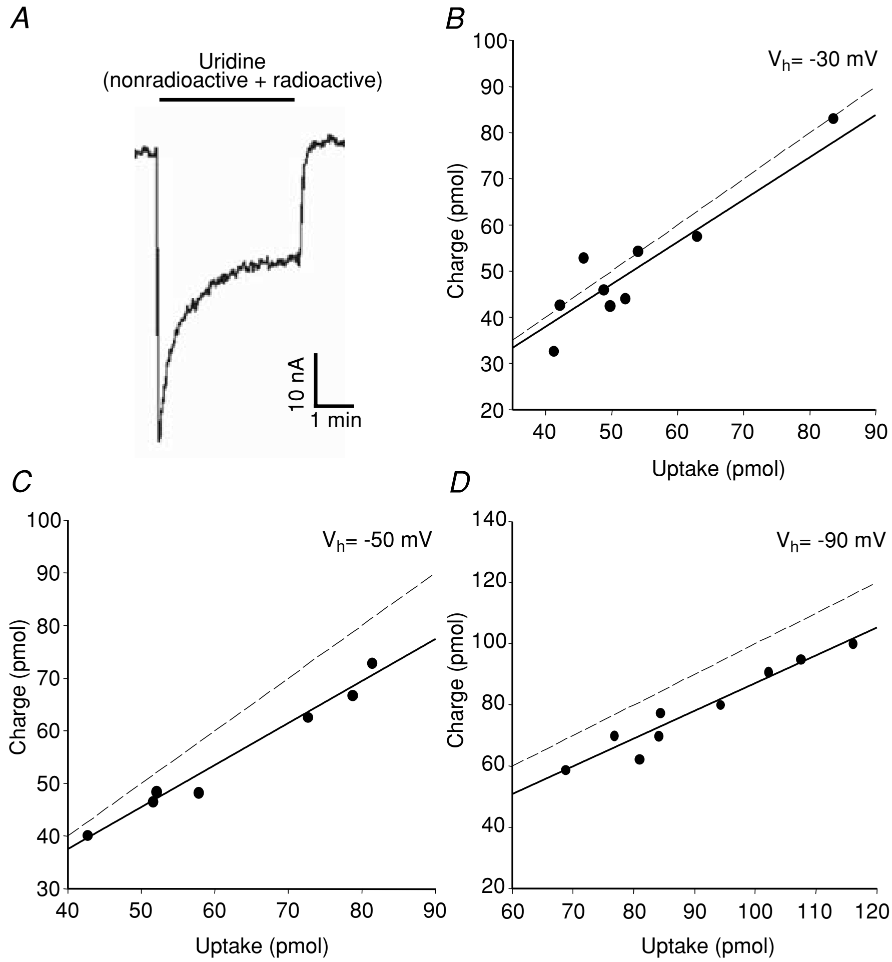

Figure 6. Stoichiometry of hCNT1

A, representative example of the current generated during application of 200 μM [^{14}C]uridine to an hCNT1-producing oocyte ($V_h = -50$ mV). *B*, hCNT1-producing oocytes were clamped at $V_h = -30$ mV and perfused with 200 μM [^{14}C]uridine. Integration of the uridine-evoked current over the uptake period (3 min) yielded the charge moved which was converted to pmoles and plotted against radiolabelled uridine uptake (pmol) in the same oocyte. The experiment was performed in 9 different oocytes. The slope (± S.E.) of the linear fit (Na^+/nucleoside ratio) is indicated by the continuous line. The dashed line indicates a slope of 1. *C*, a corresponding experiment at $V_h = -50$ mV ($n = 7$). *D*, a corresponding experiment at $V_h = -90$ mV ($n = 9$). Linear fits were not forced through zero. The expression vector was pGEM-HE.

1999) may also be important in CNT–permeant interactions. While inhibitor-sensitivity assays have revealed potential hydrogen bonds formed between hCNT1 and uridine C(3′)-OH, C(5′)-OH and N(3)-H (Zhang *et al.* 2003), the present results showing inward currents for 2′,3′-dideoxyuridine, zidovudine, zalcitabine, β-DFP-5M and β-DFP-5I demonstrate that C(3′)-OH and N(3)–H interactions are not obligatory for transport.

Na^+-dependent cotransporters are found mostly in animal cells, whereas H^+-dependent cotransporters are widely distributed in plants, bacteria and animals. A number of cotransporters utilize more than one cation. For example, the Na^+–glucose cotransporters SGLT1 and SGLT2 are able to couple sugar transport to the electrochemical gradients of Na^+, Li^+ or H^+ (Hirayama *et al.* 1994; Mackenzie *et al.* 1996*b*), and the bacterial melibiose transporter utilizes Na^+ or H^+ to drive melibiose transport (Tsuchiya & Wilson, 1978; Bassilana *et al.* 1987). In contrast, hCNT1 did not demonstrate detectable nucleoside transport when Na^+ was replaced with H^+, a behaviour that is different from hCNT3 and mCNT3 which are able to use the electrochemcial gradient of either Na^+ or H^+ to accumulate nucleosides within cells (KM Smith, SK Loewen, E Karpinski & JD Young, unpublished observations). CNTs from *C. albicans* (CaCNT), *C. elegans* (CeCNT3) and *E. coli* (NupC) function exclusively as H^+-dependent nucleoside cotransporters. Some protozoan and plant ENT family members differ from their mammalian counterparts and are also H^+-coupled (Mohlmann *et al.* 2001; Stein *et al.* 2003). Analysis of hCNT1 steady-state kinetics revealed

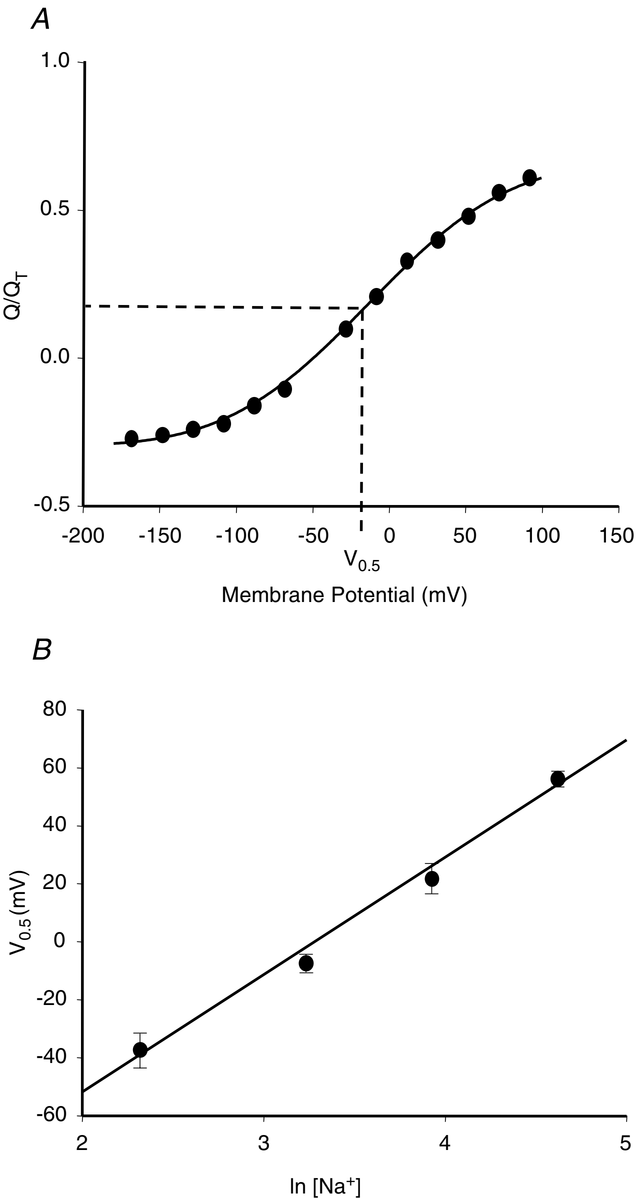

Figure 7. Dependence of hCNT1 presteady-state currents on external Na^+
A, representative charge-voltage (*Q/V*) plot for an hCNT1-producing oocyte in the presence of 25 mM external Na^+ (pH 7.5). At each clamped voltage, integration of the hCNT1 current (OFF response) with time yielded the charge (*Q*) moved within the membrane electric field. Data were normalized to Q_T, plotted as a function of voltage and fitted to the Boltzmann equation to determine z_d and $V_{0.5}$. The dashed line indicates $V_{0.5}$. *B*, mean values for $V_{0.5}$ in mV (± S.E.M.) for groups of 5 individual oocytes are plotted *versus* log [Na^+]. The fitted line corresponds to a voltage shift of 41 ± 1 mV for an e-fold change in Na^+ concentration. The expression vector was pGEM-HE.

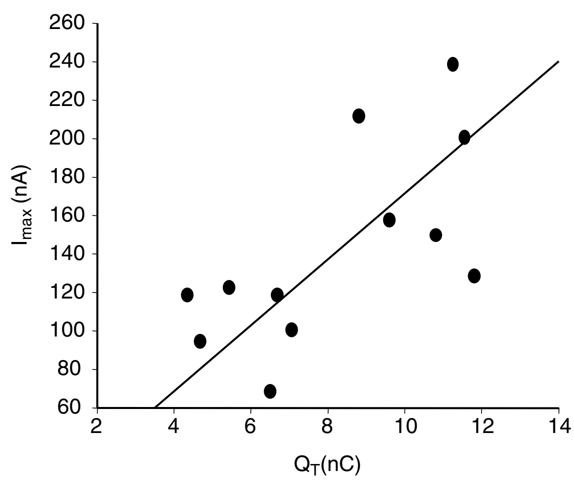

Figure 8. Turnover rate of recombinant hCNT1
The total charge (Q_T) displaced for the OFF response during voltage steps from $V_h = -50$ mV to V_t ranging from −170 to +150 mV (40 mV increments) was correlated with hCNT1 transport activity in the same cell determined as steady-state currents induced by 100 μM uridine superfusion at $V_h = -50$ mV. Linear regression analysis of results for 12 individual oocytes gave a slope of $17.2 \pm 4.4\ s^{-1}$ (continuous line), corresponding to an hCNT1 uridine turnover rate of $9.6 \pm 2.5\ s^{-1}$. The expression vector was pGEM-HE.

that Na^+ binds to the transporter first, followed by nucleoside.

Na^+–nucleoside coupling ratios for members of the CNT family have previously been determined indirectly from Hill-type analyses of relationships between nucleoside fluxes and Na^+ concentration. For example, Na^+–nucleoside coupling ratios of 1 : 1 have been proposed for recombinant rCNT1 transport of both adenosine and uridine (Yao *et al.* 1996*b*), and similar ratios have been found in studies of Na^+-dependent *cit* and *cif* nucleoside transport in renal brush-border membrane vesicles (Lee *et al.* 1988; Williams & Jarvis, 1991). Since Hill analysis of Na^+ activation curves does not determine the number of Na^+ ions that actually enter the cell as a result of transport activity (Weiss, 1997), we utilized simultaneous measurement of hCNT1-specific currents and radioactive nucleoside uptake from individual oocytes under voltage-clamp conditions to determine this parameter directly. When charge was converted to picomoles, the ratio of charge to nucleoside uptake for hCNT1 yielded a stoichiometry of 1 : 1 that was independent of membrane potential. Therefore, both direct and indirect methods agree on a Na^+–nucleoside coupling ratio of 1 : 1. These results differ from those of Larráyoz *et al.* (2004) who incorrectly reported a Na^+–nucleoside stoichiometry of 2 : 1. Examination of Fig. 6*A* of that paper reveals an apparent scaling error. A 1 : 1 Na^+–nucleoside stoichiometry for hCNT1 contrasts with parallel studies of hCNT3, where the coupling ratio approached 2 : 1 as the membrane was hyperpolarized (KM Smith, SK Loewen, E Karpinski & JD Young, unpublished observations). In this respect, CNTs resemble some other transporter families. For example, SGLT transporters have Na^+–glucose coupling ratios of either 1 : 1 (SGLT2) or 2 : 1 (SGLT1/3) (Chen *et al.* 1995; Mackenzie *et al.* 1996*b*, 1998; Diez-Sampedro *et al.* 2001). The PEPT1 and PEPT2 proton-linked peptide transporters also have different H^+–peptide coupling ratios of 1 : 1 and 2 : 1, respectively (Chen *et al.* 1999). While the stoichiometry of hCNT1 was independent of membrane potential, transport of uridine increased at more negative potentials, a finding consistent with earlier experiments in isolated rat hepatocytes (Gomez-Angelats *et al.* 1996).

Phloridzin is a potent inhibitor of SGLT1-3 (Lee *et al.* 1994; Mackenzie *et al.* 1996*b*; Hirayama *et al.* 2001) that has also been shown to reduce intestinal and renal Na^+-dependent nucleoside transport activity (Lee *et al.* 1988; Huang *et al.* 1993). In the present study, phloridzin functioned as a partial hCNT1 inhibitor with an IC_{50} of 0.2 mM, a value similar to that observed in parallel studies of hCNT3 (0.3 mM) (KM Smith, AML Ng, SYM Yao, E Karpinski & JD Young, unpublished observation). Thus, phloridzin appears to be a general CNT inhibitor. Phloridzin effects on hCNT1 uridine and Na^+ steady-state kinetics were consistent with mixed non-competitive inhibition and uncompetitive inhibition, respectively (Dixon & Webb 1958; Wong, 1975), suggesting that phloridzin binds to hCNT1 after Na^+ at a site possibly overlapping with, but not identical to, that occupied by uridine. Similarly, phloridzin binding to SGLT1 is Na^+-dependent (Vick *et al.* 1973; Lin & Hahn, 1983; Parent *et al.* 1992*a*,*b*) and competitive with glucose (Wielert-Badt *et al.* 2000; Hirayama *et al.* 2001; Novakova *et al.* 2001).

In the absence of nucleoside, and in response to step-wise changes in membrane potential, oocytes producing hCNT1 exhibited slow current relaxations (presteady-state currents) in the presence and absence of Na^+ similar to those observed for several other Na^+- or H^+-coupled cotransporters produced in *Xenopus* oocytes (Parent *et al.* 1992*a*,*b*; Loo *et al.* 1993; Mager *et al.* 1993; Chen *et al.* 1996; Klamo *et al.* 1996; Mackenzie *et al.* 1996*a*,*b*; Eskandari *et al.* 1997; Hazama *et al.* 1997; Chen *et al.* 1999). hCNT1 current–time integrals obeyed a Boltzmann function and were used to provide quantitative estimates of the fraction of the membrane field sensed by Na^+ (61%), the valency of the movable charge (−0.81), and the average number of transporters present in the oocyte plasma membrane (6.8×10^{10} per cell). The first of these parameters reflects the location of the Na^+ binding site within the hCNT1 translocation cleft. A valency of −0.81 is consistent with the determined Na^+–nucleoside coupling ratio of 1 : 1, while the estimate of hCNT1 membrane abundance allows determination, for the first time, of the turnover rate (turnover number) of a member of the CNT protein family. The calculated hCNT1 turnover rate of 9.6 uridine molecules transported per hCNT1 protein per second at −50 mV is similar to that of other cotransporters such as GAT1 (Mager *et al.* 1993) and SGLT1 (Panayotova-Heiermann *et al.* 1994), but is much lower than the mammalian ENT uridine transporter turnover rate of $10^4\ s^{-1}$ determined from NBMPR binding studies (Young & Jarvis, 1983; Cass, 1995). Table 1 lists turnover rates for other hCNT1 permeants characterized in the present study.

In conclusion, the present studies provide important new mechanistic insights into hCNT1 transport of both physiological nucleosides, including adenosine, and anticancer and antiviral nucleoside drugs. This information will guide the development of detailed kinetic models of CNT-mediated Na^+–nucleoside cotransport, and provides a functional framework to interpret CNT mutagenesis studies. Turnover rates can be combined with immunohistochemical patterns of protein expression to predict *in situ* hCNT1 fluxes of nucleosides and nucleoside drugs in normal and clinical human samples.

References

Acimovic Y & Coe IR (2002). Molecular evolution of the equilibrative nucleoside transporter family: identification of novel family members in prokaryotes and eukaryotes. *Mol Biol Evol* **19**, 2199–2210.

Baldwin SA, Beal PR, Yao SY, King AE, Cass CE & Young JD (2004). The equilibrative nucleoside transporter family, SLC29. *Pflugers Arch* **447**, 735–743.

Baldwin SA, Mackey JR, Cass CE & Young JD (1999). Nucleoside transporters: molecular biology and implications for therapeutic development. *Mol Med Today* **5**, 216–224.

Bassilana M, Pourcher T & Leblanc G (1987). Facilitated diffusion properties of melibiose permease in *Escherichia coli* membrane vesicles. Release of co-substrates is rate limiting for permease cycling. *J Biol Chem* **262**, 16865–16870.

Birnir B, Loo DDF & Wright EM (1991). Voltage-clamp studies of the Na^+/glucose cotransporter cloned from rabbit small intestine. *Pflugers Arch* **418**, 79–85.

Cass CE (1995). In *Drug Transport in Antimicrobial and Anticancer Chemotherapy*, ed. Georgopapadakou NH. Marcel Dekker, New York, NY, USA.

Che M, Ortiz DF & Arias IM (1995). Primary structure and functional expression of a cDNA encoding the bile canalicular, purine-specific Na^+ nucleoside cotransporter. *J Biol Chem* **270**, 13596–13599.

Chen XZ, Coady MJ, Jackson F, Bertleoot A & Lapointe JY (1995). Thermodynamic determination of the Na^+: glucose coupling ratio for the human SGLT1 cotransporter. *Biophys J* **69**, 2405–2414.

Chen XZ, Coady MJ & Lapointe JY (1996). Fast voltage clamp discloses a new component of presteady-state currents from the Na(+)-glucose cotransporter. *Biophys J* **71**, 2544–2552.

Chen XZ, Shayakul C, Berger UV, Tian W & Hediger MA (1998). Characterization of a rat Na^+-dicarboxylate cotransporter. *J Biol Chem* **273**, 20972–20981.

Chen XZ, Zhu T, Smith DE & Hediger MA (1999). Stoichiometry and kinetics of the high-affinity H^+-coupled peptide transporter PepT2. *J Biol Chem* **274**, 2773–2779.

Craig JE, Zhang Y & Gallagher MP (1994). Cloning of the *nupC* gene of *Escherichia coli* encoding a nucleoside transport system, and identification of an adjacent insertion element, IS 186. *Mol Microbiol* **11**, 1159–1168.

Crawford CR, Patel DH, Naeve C & Belt JA (1998). Cloning of the human equilibrative, nitrobenzylmercaptopurine riboside (NBMPR)-insensitive nucleoside transporter *ei* by functional expression in a transport-deficient cell line. *J Biol Chem* **273**, 5288–5293.

de Koning HP & Jarvis SM (1999). Adenosine transporters in bloodstream forms of *Trypanosoma brucei brucei*: Substrate recognition motifs and affinity for trypanocidal drugs. *Mol Pharmacol* **56**, 1162–1170.

Diez-Sampedro A, Eskandari S, Wright EM & Hirayama BA (2001). Na^+-to-sugar stoichiometry of SGLT3. *Am J Physiol Renal Physiol* **49**, F278–F282.

Dixon M & Webb E (1958). In *Enzymes*, ed. Longmans WI. Green, Ltd, London, England.

Dresser MJ, Gerstin KM, Gray AT, Loo DF & Giacomini KM (2000). Electrophysiological analysis of the substrate selectivity of a sodium-coupled nucleoside transporter (rCNT1) expressed in *Xenopus laevis* oocytes. *Drug Metab Dispos* **28**, 1135–1140.

Eskandari S, Loo DDF, Dai G, Levy O, Wright EM & Carrasco N (1997). Thyroid Na^+/I^- symporter. *J Biol Chem* **272**, 27230–27238.

Fang X, Parkinson FE, Mowles DA, Young JD & Cass CE (1996). Functional characterization of a recombinant sodium-dependent nucleoside transporter with selectivity for pyrimidine nucleosides ($CNT1_{rat}$) by transient expresssion in cultured mammalian cells. *Biochem J* **317**, 457–465.

Fredholm BB (1997). Adenosine and neuroprotection. *Int Rev Neurobiol* **40**, 259–280.

Gomez-Angelats M, Del Santo B, Mercader J, Ferrer-Martinex A, Felipe A, Casado J & Pastor-Anglada M (1996). Hormonal regulation of concentrative nucleoside transport in liver parenchymal cells. *Biochem J* **313**, 915–920.

Graham KA, Leithoff J, Coe IR, Mowles D, Mackey JR, Young JD & Cass CE (2000). Differential transport of cytosine-containing nucleosides by recombinant human concentrative nucleoside transporter protein hCNT1. *Nucleosides Nucleotides Nucl Acids* **19**, 415–434.

Griffiths DA & Jarvis SM (1996). Nucleoside and nucleobase transport systems of mammalian cells. *Biochim Biophys Acta* **1286**, 153–181.

Hamilton SR, Yao SYM, Ingram JC, Hadden DA, Ritzel MWL, Gallagher MP, Henderson PJF, Cass CE, Young JD & Baldwin SA (2001). Subcellular distribution and membrane topology of the mammalian concentrative Na^+-nucleoside cotransporter rCNT1. *J Biol Chem* **276**, 27981–27988.

Handschumacher RE, Pizzorno GL & Cheng CY (2000). In *Cancer Metabolism*, ed. Bast DC Jr, Kufe DW, Pollack RR, Weichselbaum RR, Holland JR & Frei E III, pp. 625–648. BC Decker Inc., Hamilton, ON, Canada.

Hazama A, Loo DDF & Wright EM (1997). Presteady-state currents of the rabbit Na^+/glucose cotransporter (SGLT1). *J Membr Biol* **155**, 175–186.

Hirayama BA, Diez-Sampedro A & Wright EM (2001). Common mechanisms of inhibition for the Na^+/glucose (hSGLT1) and Na^+/Cl^-/GABA (hGAT1) cotransporters. *Br J Pharmacol* **134**, 484–495.

Hirayama BA, Loo DDF & Wright EM (1994). Protons drive sugar transport through the Na^+/glucose cotransporter (SGLT1). *J Biol Chem* **269**, 21407–21410.

Huang Q-Q, Harvey CM, Paterson ARP, Cass CE & Young JD (1993). Functional expression of Na^+-dependent nucleoside transport systems of rat intestine in isolated oocytes of *Xenopus laevis*: Demonstration that rat jejunum expresses the purine-selective system N1 (*cif*) and a second, novel system N3 having broad specificity for purine and pyrimidine nucleosides. *J Biol Chem* **268**, 20613–20619.

Huang Q-Q, Yao SYM, Ritzel MWL, Paterson ARP, Cass CE & Young JD (1994). Cloning and functional expression of a complementary DNA encoding a mammalian nucleoside transport protein. *J Biol Chem* **269**, 17757–17760.

Hyde RJ, Cass CE, Young JD & Baldwin SA (2001). The ENT family of eukaryote nucleoside and nucleobase transporters: recent advances in the investigation of structure/function relationships and the identification of novel isoforms. *Mol Membr Biol* **18**, 53–63.

Jauch P & Lauger P (1986). Electrogenic properties of the sodium-alanine cotransporter in pancreatic acinar cells. II. Comparison with transport models. *J Membr Biol* **94**, 117–127.

Klamo EM, Drew ME, Landfear SM & Kavanaugh MP (1996). Kinetics and stoichiometry of a proton/*myo*-inositol cotransporter. *J Biol Chem* **271**, 14937–14943.

Larráyoz IM, Casado FJ, Pastor-Anglada M & Lostao MP (2004). Electrophysiological characterization of the human Na^+/nucleoside cotransporter 1 (hCNT1) and role of adenosine on hCNT1 function. *J Biol Chem* **279**, 8999–9007.

Lee CW, Cheeseman CI & Jarvis SM (1988). Na^+- and K^+-dependent uridine transport in rat renal brush-border membrane vesicles. *Biochim Biophys Acta* **942**, 139–149.

Lee W-S, Kanai Y, Wells RG & Hediger MA (1994). The high affinity Na^+/glucose cotransporter. Re-evaluation of function and distribution of expression. *J Biol Chem* **269**, 12032–12039.

Liman ER, Tytgat J & Hess P (1992). Subunit of stoichiometry of a mammalian K^+ channel determined by construction of multimeric cDNAs. *Neuron* **9**, 861–871.

Lin JT & Hahn K-D (1983). Synthesis of ^{3}H-phloridzin and its binding behaviour to renal brush border membranes. *Anal Biochem* **129**, 337–344.

Loewen SK, Ng AM, Mohabir NN, Baldwin SA, Cass CE & Young JD (2003). Functional characterization of a H^+/nucleoside co-transporter (CaCNT) from *Candida albicans*, a fungal member of the concentrative nucleoside transporter (CNT) family of membrane proteins. *Yeast* **20**, 661–675.

Loewen SK, Ng AM, Yao SY, Cass CE, Baldwin SA & Young JD (1999). Identification of amino acid residues responsible for the pyrimidine and purine nucleoside specificities of human concentrative Na^+ nucleoside cotransporters hCNT1 and hCNT2. *J Biol Chem* **274**, 24475–24484.

Loo DDF, Hazama A, Supplisson S, Turk E & Wright EM (1993). Relaxation kinetics of the Na^+/glucose cotransporter. *Proc Natl Acad Sci* **90**, 5767–5771.

Lostao MP, Mata JF, Larráyoz IM, Inzillo SM, Casado FJ & Pastor-Anglada M (2000). Electrogenic uptake of nucleosides and nucleoside-derived drugs by the human nucleoside transporter 1 (hCNT1) expressed in *Xenopus laevis* oocytes. *FEBS Lett* **481**, 137–140.

Mackenzie B, Loo DDF, Fei Y-J, Liu WJ, Ganapathy V, Leibach FH & Wright EM (1996*a*). Mechanisms of the human intestinal H^+-coupled oligopeptide transporter hPEPT1. *J Biol Chem* **271**, 5430–5437.

Mackenzie B, Loo DDF, Panayotova-Heiermann M & Wright EM (1996*b*). Biophysical characteristics of the pig kidney Na^+/glucose cotransporter SGLT2 reveal a common mechanism for SGLT1 and SGLT2. *J Biol Chem* **271**, 32678–32683.

Mackenzie B, Loo DDF & Wright EM (1998). Relationships between Na^+/glucose cotransporter (SGLT1) currents and fluxes. *J Membr Biol* **162**, 101–106.

Mackey JR, Baldwin SA, Young JD & Cass CE (1998). Nucleoside transport and its significance for anticancer drug resistance. *Drug Resist Updat* **1**, 310–324.

Mackey JR, Yao SY, Smith KM, Karpinski E, Baldwin SA, Cass CE & Young JD (1999). Gemcitabine transport in *Xenopus* oocytes expressing recombinant plasma membrane mammalian nucleoside transporters. *J Natl Cancer Inst* **91**, 1876–1881.

Mager S, Naeve J, Quick M, Labarca C, Davidson N & Lester HA (1993). Steady states, charge movements, and rates for a cloned GABA transporter expressed in *Xenopus* oocytes. *Neuron* **10**, 177–188.

Mohlmann T, Mezher Z, Schwerdtfeger G & Neuhaus HE (2001). Characterization of a concentrative type of adenosine transporter from *Arabidopsis thaliana* (ENT1,At). *FEBS Lett* **509**, 370–374.

Novakova R, Homerova D, Kinne RKH, Kinne-Saffran E & Lin JT (2001). Identification of a region critically involved in the interaction of phloridzin with the rabbit sodium-D-glucose cotransporter SGLT1. *J Membr Biol* **184**, 55–60.

Panayotova-Heiermann M, Loo DDF, Lostao MP & Wright EM (1994). Sodium/D-glucose cotransporter charge movements involve polar residues. *J Biol Chem* **269**, 21016–21020.

Panayotova-Heiermann M, Loo DDF & Wright EM (1995). Kinetics of steady-state currents and charge movements associated with the rat Na^+/glucose cotransporter. *J Biol Chem* **270**, 27099–27105.

Parent L, Supplisson S, Loo DD & Wright EM (1992*a*). Electrogenic properties of the cloned Na^+/glucose cotransporter: Part I. Voltage-clamp studies. *J Membr Biol* **125**, 49–62.

Parent L, Supplisson S, Loo DD & Wright EM (1992*b*). Electrogenic properties of the cloned Na^+/glucose cotransporter: Part II. A transport model under non-rapid equilibrium conditions. *J Membr Biol* **125**, 63–79.

Perigaud C, Aubertin AM, Benzaria S, Pelicano H, Girardet JL, Maury G, Gosselin G, Kirn A & Imbach JL (1994). Equal inhibition of the replication of human immunodeficiency virus in human T-cell culture by ddA bis (SATE) phosphotriester and 3′-azido-2′,3′-dideoxythymidine. *Biochem Pharmacol* **48**, 11–14.

Ritzel MW, Ng AM, Yao SY, Graham K, Loewen SK, Smith KM, Ritzel RG, Mowles DA, Carpenter P, Chen XZ, Karpinski E, Hyde RJ, Baldwin SA, Cass CE & Young JD (2001). Molecular identification and characterization of novel human and mouse concentrative Na^+-nucleoside cotransporter proteins (hCNT3 and mCNT3) broadly selective for purine and pyrimidine nucleosides (system *cib*). *J Biol Chem* **276**, 2914–2927.

Ritzel MW, Yao SY, Huang M-Y, Elliot JF, Cass CE & Young JD (1997). Molecular cloning and functional expression of cDNAs encoding a human Na^+-nucleoside cotransporter (hCNT1). *Am J Physiol Cell Physiol* **272**, C707–C714.

Ritzel MW, Yao SY, Ng AM, Mackey JR, Cass CE & Young JD (1998). Molecular cloning, functional expression and chromosomal localization of a cDNA encoding a human Na^+ nucleoside cotransporter (hCNT2) selective for purine nucleosides and uridine. *Mol Membr Biol* **15**, 203–211.

Shryock JC & Belardinelli L (1997). Adenosine and adenosine receptors in the cardiovascular system: biochemistry, physiology, and pharmacology. *Am J Cardiol* **79**, 2–10.

Stein A, Vaseduvan G, Carter NS, Ullman B, Landfear SM & Kavanaugh MP (2003). Equilibrative nucleoside transporter family members from *Leishmania donovani* are electrogenic proton symporters. *J Biol Chem* **278**, 35127–35134.

Stein WD (1990). *Channels, Carriers, and Pumps: an Introduction to Membrane Transport*, pp. 173. Academic Press Inc, San Diego, CA, USA.

Tsuchiya T & Wilson TH (1978). Cation-sugar cotransport in the melibiose transport system of *Escherichia coli*. *Membr Biochem* **2**, 63–79.

Vick H, Diedrich DF & Baumann K (1973). Reevaluation of renal tubular glucose transport inhibition by phloridzin analogs. *Am J Physiol* **224**, 552–557.

Wadiche JI, Arriza JL, Amara SG & Kavanaugh MP (1995). Kinetics of a human glutamate transporter. *Neuron* **14**, 1019–1027.

Wang J, Su S-F, Dresser MJ, Schaner ME, Washington CB & Giacomini KM (1997). Na^+-dependent purine nucleoside transporter from human kidney: cloning and functional characterization. *Am J Physiol Renal Physiol* **273**, F1058–F1065.

Wang ZX, Duan W, Wiebe LI, Balzarini J, De Clercq E & Knauss EE (2001). Synthesis of 1-(2-deoxy-beta-D-ribofuranosyl)-2,4-difluoro-5-substituted-benzene thymidine mimics, some related alpha-anomers, and their evaluation as antiviral and anticancer agents. *Nucleosides Nucleotides Nucl Acids* **20**, 11–40.

Weiss JN (1997). The Hill equation revisited: uses and misuses. *FASEB J* **11**, 835–841.

Wielert-Badt S, Lin JT, Lorenz M, Fritz S & Kinne RK (2000). Probing the conformation of the sugar transport inhibitor phlorizin by 2D-NMR, molecular dynamics studies, and pharmacophore analysis. *J Med Chem* **43**, 1692–1698.

Williams TC & Jarvis SM (1991). Multiple sodium-dependent nucleoside transport systems in bovine renal brush-border membrane vesicles. *Biochem J* **274**, 27–33.

Wong J (1975). In *Kinetics of Enzyme Mechanisms*. Academic Press Inc., New York, NY, USA.

Wright EM, Loo DD, Panayotova-Heiermann M & Boorer KJ (1994). Mechanisms of Na^+-glucose cotransport. *Biochem Soc Trans* **22**, 646–650.

Xiao G, Wang J, Tangen T & Giacomini KM (2001). A novel proton-dependent nucleoside transporter, CeCNT3, from *Caenorhabditis elegans*. *Mol Pharmacol* **59**, 339–348.

Yao SYM, Cass CE & Young JD (1996*a*). Transport of the antiviral nucleoside analogs 3′-azido-3′-deoxythymidine (AZT) and 2′,3′-dideoxycytidine (ddC) by a recombinant nucleoside transporter (rCNT) expressed in *Xenopus* oocytes. *Mol Pharmacol* **50**, 388–393.

Yao SYM, Ng AML, Loewen SK, Cass CE, Baldwin SA & Young JD (2002*a*). An ancient prevertebrate Na^+-nucleoside cotransporter (hfCNT) from the Pacific hagfish (*Eptatretus stouti*). *Am J Physiol Cell Physiol* **283**, C155–C168.

Yao SY, Ng AM, Ritzel MW, Gati WP, Cass CE & Young JD (1996*b*). Transport of adenosine by recombinant purine- and pyrimidine-selective sodium/nucleoside cotransporters from rat jejunum expressed in *Xenopus laevis* oocytes. *Mol Pharmacol* **50**, 1529–1535.

Yao SY, Ng AM, Sundaram M, Cass CE, Baldwin SA & Young JD (2001). Transport of antiviral 3′-deoxy-nucleoside drugs by recombinant human and rat equilibrative, nitrobenzylthioinosine (NBMPR)-insensitive (ENT2) nucleoside transporter proteins produced in *Xenopus* oocytes. *Mol Membr Biol* **18**, 161–167.

Yao SY, Ng AM, Vickers MF, Sundaram M, Cass CE, Baldwin SA & Young JD (2002*b*). Functional and molecular characterization of nucleobase transport by recombinant human and rat equilibrative nucleoside transporters 1 and 2. Chimeric constructs reveal a role for the ENT2 helix 5–6 region in nucleobase translocation. *J Biol Chem* **277**, 24938–24948.

Young JD, Cheeseman CI, Mackey JR, Cass CE & Baldwin SA (2001). Molecular mechanisms of nucleoside and nucleoside drug transport. *Current Top Membr* **50**, 329–378.

Young JD & Jarvis SM (1983). Nucleoside transport in animal cells. *Biosci Rep* **3**, 309–322.

Zhang J, Visser F, Vickers MF, Lang T, Robins MJ, Nielsen LPC, Nowak I, Baldwin SA, Young JD & Cass CE (2003). Uridine binding motifs of human concentrative nucleoside transporters 1 and 3 (hCNT1 and hCNT3) produced in *Saccharomyces cerevisiae*. *Mol Pharmacol* **64**, 1512–1520.

Acknowledgements

This work was supported by the National Cancer Institute of Canada, with funds from the Canadian Cancer Society, the Heart and Stroke Foundation, Canada, the Canadian Institutes of Health Research, and the Medical Research Council, UK. J.D.Y. is Heritage Scientist of the Alberta Heritage Foundation for Medical Research. C.E.C. is a Canada Research Chair in Oncology at the University of Alberta.

Supplementary material

The online version of this paper can be accessed at: DOI: 10.1113/jphysiol.2004.068189
http://jp.physoc.org/cgi/content/full/jphysiol.2004.068189/DC1 and contains 10 supplementary figures, Figs S1–S10, examining steady-state and presteady-state currents of hCNT1.
This material can also be found at:
http://www.blackwellpublishing.com/products/journals/suppmat/tjp/tjp374/tjp374sm.htm